Journal of Biomedical Optics 8(2), 308–315 (April 2003)

Quantitative analysis of near-infrared tomography: sensitivity to the tissue-simulating precalibration phantom

Shudong Jiang
Brian W. Pogue
Troy O. McBride
Keith D. Paulsen
Dartmouth College
Thayer School of Engineering
Hanover, New Hampshire 03755
Shudong.Jiang@Dartmouth.edu

Abstract. A near-infrared (NIR) imaging system is evaluated as a diagnostic clinical tool to image total hemoglobin concentration and oxygen saturation within tissue. Calibration of this type of system requires measurement of the response at each detector and source location from a homogeneous tissue-simulating phantom. The effect of using calibration phantoms of varying composition, size, and optical properties is examined to determine how it affects the overall image accuracy. All of the calibration phantoms investigated result in accurate reconstruction of absorbing heterogeneities due to increased blood concentration with less than 4% standard deviation. Images from a patient with a biopsy-confirmed ductal carcinoma are also evaluated and found to be insensitive to the choice of calibration object, with only 1% variation between images generated with different calibration objects. The tumor total hemoglobin contrast is approximately 240% higher than the average total hemoglobin concentration in contralateral breast. Soft calibration phantoms, which mimic the elastic properties of human breast tissue, are also considered and found to diminish positioning errors in the fibers relative to the actual breast exam, thereby reducing the artifacts in the periphery of the reconstructed image.
[DOI: 10.1117/1.1559692]

Keywords: near-infrared; tomography; breast cancer; tissue phantom; photon migration.

Paper 1074 received Nov. 8, 2001; revised manuscript received May 29, 2002; accepted for publication Sep. 23, 2002.

1 Introduction

Near-infrared tomographic imaging is being investigated clinically as a possible noninvasive method for imaging hemoglobin.[1] It can provide noninvasive characterization of tumors *in vivo*,[2–4] and as this modality progresses toward clinical implementation, issues related to system design,[5,6] calibration,[7–9] accuracy, and precision,[10] need to be addressed. In particular, as parallel acquisition from multiple detectors becomes a useful technique, it will be imperative to have a method to normalize all source and detector strengths. This is needed to remove systematic offsets that occur because multiple fiber optics and detectors are used to record the measured data.[7,11] While parallel data acquisition has been shown to work in practice,[7] issues related to proper calibration have not been systematically evaluated. The quantitative effect of different calibration objects is examined here for its influence on resulting images. We investigate an approach to system calibration that utilizes breast-tissue mimicking phantoms to provide an accurate daily accounting of the system offsets at multiple channels in parallel.

In the tomographic imaging method used here, theoretical predictions of light diffusion in tissue are computed to match the measured transmission values at multiple projection locations through the breast. High-frequency (100 MHz) intensity waves propagate through the tissue, allowing the detection of both an amplitude and phase shift relative to the wavefront launched from the source. Using a nonlinear least-squares minimization between the predicted and measured transmission data, simultaneous images of absorption and scattering coefficients can be recovered through an iterative solution to a regularized matrix equation following the Newton-Raphson method.[12–14] The tissue can be characterized by deriving concentration images of oxyhemoglobin, deoxyhemoglobin, and water from the absorption and scattering coefficient images reconstructed at multiple wavelengths.[15] In our studies, a multiparameter concentration fit at each point in the image has been used to deconvolve the total absorption coefficient spectrum into these constituents.[15] Since the optical fluence is nonlinear with respect to the interaction coefficients (i.e., optical properties), significant calibration issues can arise when using a model-based image reconstruction approach. The nonlinear dependence of the measurements on the optical properties can be reduced by using the logarithm of the amplitude. In addition, many system calibrations that can be ignored in qualitative imaging require more attention to achieve quantitative imaging of total hemoglobin concentrations on an absolute scale.

We have adopted a homogeneous phantom calibration procedure to provide a measure of system response at all source-

1083-3668/2003/$15.00 © 2003 SPIE

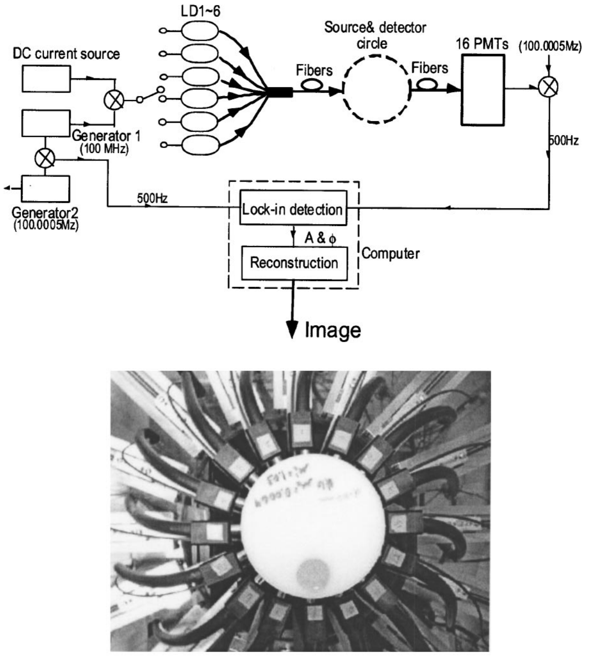

Fig. 1 Schematic diagram of (a) the system and (b) the source detector fiber optic interface.

detector measurement projections, and demonstrated that the calibration homogeneous phantom can be used to improve the reconstruction quality and give the good match of the absolute value.[7] Attempts to reconstruct images without any calibration have ended in complete failure of the imaging algorithm, resulting in images that are all noise from systematic errors. Thus in the experience of the current system development, calibration of the data is an essential step in the data processing, prior to reconstruction. However, it is not clear if the use of a calibration phantom depends on having a good match to the optical properties and size of the tissue to be imaged. In particular, large differences between the calibration object and the tissue being imaged may result in errors that cannot be eliminated. A range of homogenous phantoms with different characteristics (e.g., size and optical properties) was used to determine the stability of this calibration approach for quantitatively accurate imaging of tissue. In addition, the issue of having intimate coupling from an optical fiber contacting a hard tissue phantom has always been problematic, so in this study we also examine the potential of using softer phantoms, which have similar stiffness, or elastic properties, to breast tissue, as a means to better measure the source-detector coupling. The consistency of the calibration for the system is evaluated through phantoms with different concentration blood heterogeneities, as well as with a clinical image of a diseased breast.

2 Materials and Methods

2.1 *Imaging System*

A clinical prototype imaging system has been developed in our laboratory and is under evaluation in both tissue phantoms and patient trials.[6,8,15,16] Figure 1 shows a schematic diagram of the system along with a photograph of the source detector fiber optic interface with a tissue-simulating phantom placed in the array. The breast or phantom to be imaged is circled uniformly by an interface of 16 silica glass fibers of 1 mm diam each, and 16 detector fiber bundles of 6 mm diam each. The source fibers are paired with each detector and are translated radially toward the breast. The diameter of the circular interface of source and detector fiber optics can be changed from 66 to 200 mm by control of stepper motor stages attached to each source and detector fiber pair. Near-infrared light from six laser diodes is used serially to illuminate the region of interest with average power less than 30 mW each, having wavelengths of 661, 761, 785, 808, 826, and 849 nm. The driving current subsystem involves both dc and rf components, with the rf modulated by a function generator with the frequency of 100 MHz. The source wavelength is interchanged using a high-power rf switch for the driving current. The diffusely transmitted light is detected by 16 fiber bundles and delivered to each of 16 photomultiplier tubes that sample the signal in parallel. The electrical outputs from the photomultipliers are heterodyned down to 500 Hz, amplified filtered, and sampled by a 64-channel 200-kHz A/D board in the computer. A single measurement at all detectors for one source location requires approximately 0.5 s. The complete measurement for all six wavelengths at all source-detector pairs occurs in approximately 5 min. A complete discussion of the hardware system and its performance is described in a prior report.[8]

2.2 *Image Reconstruction*

The image reconstruction algorithm uses 256 measurements of phase shift and amplitude, together with a finite element solution of the diffusion equation to optimize the match between measured and calculated data. A schematic diagram of the algorithm for processing the data and reconstructing an image is shown in Fig. 2. The inverse solution is computed on a regular grid structure of 221 nodes, where the values of absorption and reduced scattering coefficient are evaluated.[12] To reduce the effect of nonuniformity in the fiber optics and detectors, a homogeneous phantom is measured. Then, a dataset for the reconstruction of a target heterogeneous object is calibrated as:

$$\varphi^{i}_{\mathrm{calibrated(hetero)}} = \varphi^{i}_{\mathrm{measured(hetero)}} - [\varphi^{i}_{\mathrm{measured(homo)}} - \varphi^{i}_{\mathrm{calculated(homo)}}] - \overline{\varphi}_{\mathrm{offset(net)}}, \qquad (1)$$

where $\varphi^{i}_{\mathrm{measured}}$ is the recorded signal-measured amplitude and phase at each i of the 256 measurements from the calibration phantom (homo) and the target heterogeneous object (hetero); $\varphi^{i}_{\mathrm{calculated}}$ is the corresponding calculation for the homogeneous (homo) case, while $\overline{\varphi}_{\mathrm{offset(net)}} = \overline{\varphi}_{\mathrm{offset(hetero)}} - \overline{\varphi}_{\mathrm{offset(homo)}}$ is the correction of the initial phase differences between the homogenous calibration phantom measurement and target heterogeneous object measurement resulting from long-term system drift. The offsets for both the homogeneous phantom and the target heterogeneous object measurements are estimated as:

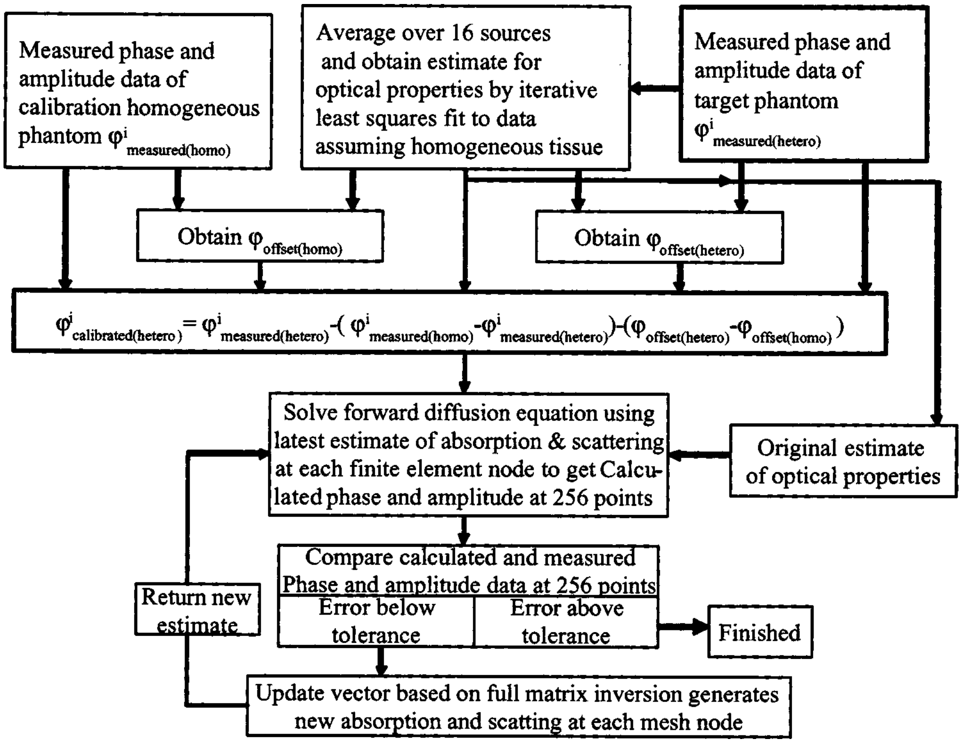

Fig. 2 Reconstruction algorithm diagram.

$$\overline{\varphi}_{\text{offset(homo)}}=\frac{\sum_{i=1}^{N}[\varphi^{i}_{\text{measured(homo)}}-\varphi^{i}_{\text{calculated(homo)}}]}{N}, \quad (2)$$

$$\overline{\varphi}_{\text{offset(hetero)}}=\frac{\sum_{i=1}^{N}[\varphi^{i}_{\text{measured(hetero)}}-\varphi^{i}_{\text{calculated(hetero)}}]}{N}, \quad (3)$$

where $\varphi^{i}_{\text{calculated(homo)}}$ and $\varphi^{i}_{\text{calculated(hetero)}}$ are calculated based on the homogeneous fitting algorithm. To determine the initial optical property estimate for the heterogeneous tissue or phantom, the measurements are averaged for each of the 16 sources, and a homogeneous fitting algorithm[7,9] is used to determine a "homogeneous" estimate of the properties that is consistent with a diffusion equation solution that matches the averaged data. In this manner, the initial estimate is determined solely from the target heterogeneous object measurements. While this "homogeneous" set of values is only approximate, it provides an excellent initial guess for the reconstruction algorithm, because it assumes that the background value is close to the true value, allowing perturbations within the field to be reconstructed. In practice, the reconstruction algorithm can still recover images of objects that are much larger than point perturbations; however, having an accurate initial guess of the spatially averaged optical properties has been found to be very important for recovering an accurate final image.

Furthermore, by using the known specific absorption of oxyhemoglobin, deoxyhemoglobin and water, images of total hemoglobin can be reconstructed by fitting data of absorption images that are acquired at multiwavelengths on a pixel-by-pixel basis.[7]

2.3 *Phantoms Used in Experiments*

Photographs of one heterogeneous phantom and six homogeneous calibration phantoms are shown in Fig. 3. Most of the breast cancers imaged in the current clinic trial have had one tumor in the imaging plane, and the absorption coefficient contrast relative to the normal tissue is high (a factor of 2 to 3 increase), so in our phantom studies, a single inclusion is used as the heterogeneous phantom. Earlier studies have looked at quantifying highly heterogeneous tissue phantoms and demonstrated that heterogeneity can decrease the ability to accurately quantify smaller objects. However, in this current study we focus on larger tumors that are typical of the size at clinical presentation (typically 1.5 cm diam average).

As shown in Figs. 3(a) and 3(b), the heterogeneous phantom consisted of 84-mm-diam material with a single hole of 20 mm diam drilled near the edge, parallel to the depth axis of the cylinder. This hole was filled with different concentrations of blood to provide a target with variable contrast. The blood used in the experiment is human blood and was kept in a 7-ml tube with liquid additive [volume: 0.07 ml of 15% solution (buffered); weight: 10.5 mg EDTA (k3)]. The total hemoglobin content in these samples of blood was 140 g/l (measured spectrophotometrically in a clinical cooximeter system). The blood was then aliquoted into a water-interlipid solution to make specific concentrations of blood solution as needed.

The phantom's optical properties were measured before the hole was drilled and were found to yield an absorption coefficient $\mu_a = 0.0064\,\text{mm}^{-1}$ and reduced scattering coefficient $\mu_s' = 1.0\,\text{mm}^{-1}$ at a light wavelength of 785 nm. The hole was filled with an intralipid and ink solution that matched the background reduced scattering coefficient and had a slightly

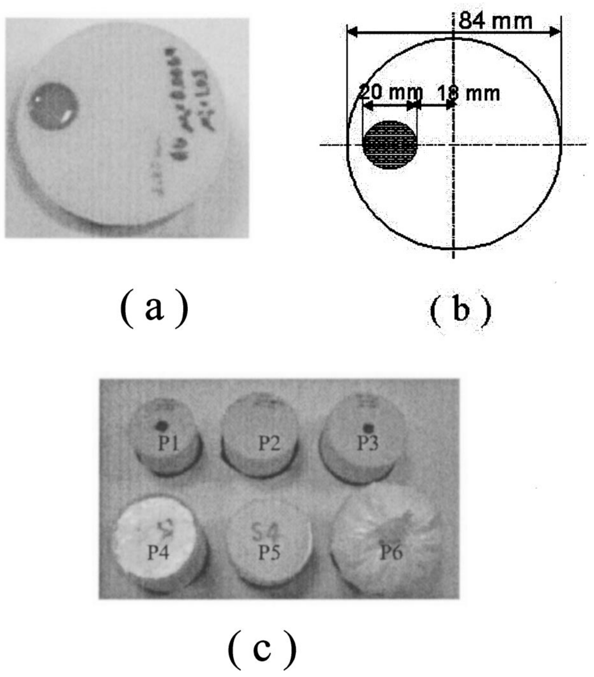

(a) (b)

(c)

Fig. 3 Photographs and sketch of the target heterogeneous and calibration phantoms. (a) Target heterogeneous phantom. (b) Sketch of the heterogeneous phantom. Diameter and height are 84 and 55 mm, respectively. Diameter of the hole is 20 mm. (c) Calibration homogeneous phantoms. P1 through P3: solid phantoms with the same height of 55 mm but different diameters of 73, 84, and 92 mm, respectively. P4 and P5: soft solid phantoms with the same diameter of 82 mm, but different heights of 80 and 52 mm, respectively. P6: Liquid phantom, i.e., a plastic storage bag with 86 mm diam in which 2% intralipid was filled.

higher absorption (0.00643 mm^{-1}) before adding different concentrations of blood. Measurements from the six homogenous phantoms were used to calibrate data recorded from the target heterogeneous phantom. Figure 3(c) shows the photograph of these six homogenous phantoms. The first three calibration phantoms were constructed from the same resin composition, and each had the same height of 55 mm but diameters of 73, 84, and 92 mm, respectively. The average optical property coefficients of these three phantoms were $\mu_a = 0.005\,\mathrm{mm}^{-1}$ and $\mu_s' = 1.0\,\mathrm{mm}^{-1}$ for P1, $\mu_a = 0.005\,\mathrm{mm}^{-1}$ and $\mu_s' = 1.3\,\mathrm{mm}^{-1}$ for P2, and $\mu_a = 0.004\,\mathrm{mm}^{-1}$ and $\mu_s' = 1.1\,\mathrm{mm}^{-1}$ for P3. Two other phantoms, P4 and P5, were constructed of a soft RTV-based material, and each had the same diameter (82 mm), but heights of 80 and 52 mm, respectively. The optical properties of the P4 and P5 phantoms were both $\mu_a = 0.004\,\mathrm{mm}^{-1}$ and $\mu_s' = 1.6\,\mathrm{mm}^{-1}$. The final phantom, P6, was a liquid composed of 2% intralipid solution in a plastic storage bag, which was compressed in the fiber array to an 86 mm diam and had optical properties of $\mu_a = 0.003\,\mathrm{mm}^{-1}$ and $\mu_s' = 1.6\,\mathrm{mm}^{-1}$.

3 Results

Figure 4 shows the absorption and reduced scattering coefficient images of the target phantom with a fixed blood concentration object, reconstructed from data calibrated against each of the six homogeneous phantoms described in the previous section. The blood concentration used for all images in Fig. 4(a) was 0.6% in the heterogeneity region, and 1% for all the images in Fig. 4(b). In these experiments, there was no significant contrast in the scattering coefficient, and the images of this optical property are relatively homogeneous in Fig. 4. The increase in absorption is readily observed in both blood concentrations examined here, with fewer artifacts appearing around the heterogeneity and in the periphery of the circular field compared with the expected uniform background around the heterogeneity region. There is some indication that the peripheral artifacts decrease when the soft calibration phantoms are used (i.e., P4 and P5), as compared to the hard calibration phantoms (i.e., P1 to P3). Images reconstructed with the liquid phantom, P6, contain the most artifact.

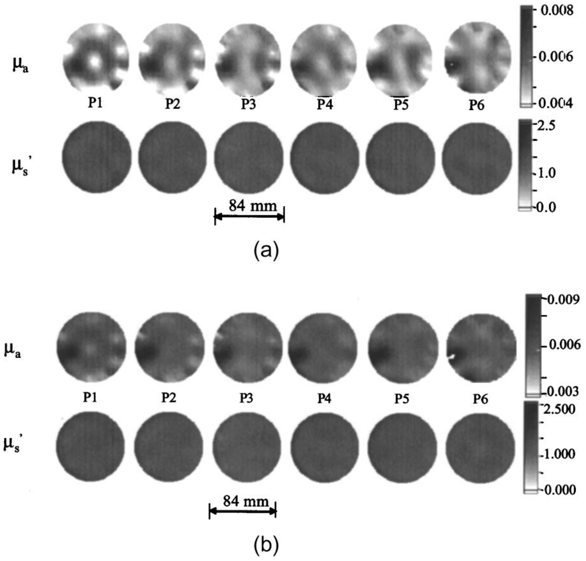

(a)

(b)

Fig. 4 Absorption and scattering images of the target phantom with blood concentrations of 0.6% and 1%, reconstructed by using different calibration phantoms P1~P6. Wavelength of the light source is 785 nm.

Figure 5 shows a plot of the estimated absorption coefficient versus blood concentration with each line of data corresponding to a different homogeneous calibration phantom. The blood concentration was changed from 0 to 1% as shown on the horizontal axis. The lines L_{P1} through L_{P6} are the linear regression fits to the values of maximum absorption coefficient within the blood region. Equations in the lower right side of the figure show the slopes of the fitted lines. The average slope for the lines was calculated along with its standard deviation. In these cases the standard deviation was 3% of the average value. The variation in the absolute reconstructed absorption coefficient for the same blood concentration is within the range of 1.4 to 3.1%. When ignoring the cases reconstructed from data calibrated using the liquid phantom (P6) and the solid hard phantom with a diameter of 73 mm (P1), the variation in the slope and the absolute absorption coefficient is reduced to within 0.6 to 1.2%.

The long-term stability of the system offset factors was investigated by measuring the two hard homogenous calibration phantoms, P2 and P3, on multiple days. These different calibration datasets were used to reconstruct the absorption coefficient images shown in Fig. 4 again. It was found that the

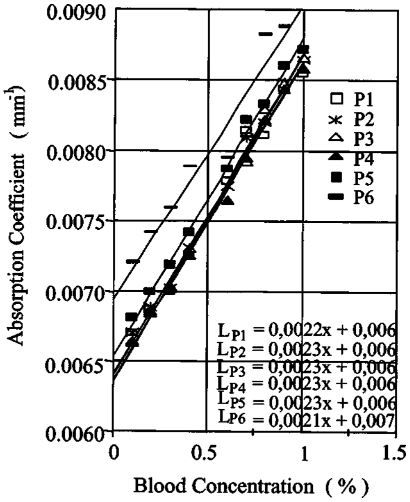

Fig. 5 Absorption coefficient versus blood concentration and calibration phantom. Lines L_{P1} through L_{P6} are fits of the reconstructed maximum absorption coefficient of the blood region that is reconstructed by using different calibration phantoms.

variation in the absolute maximum absorption coefficient was less than 1%, and there was no change in the slope of absorption coefficient versus blood concentration presented in Fig. 5.

The variation of the reconstructed reduced scattering coefficient of all cases of different blood concentrations and by all P1 through P6 calibration phantoms is estimated to be about 4%. When the data from the calibrations by P1 and P6 is eliminated, the variation of the reconstructed reduced scattering coefficient is reduced to 3%.

To evaluate the accuracy of the absolute value of absorption coefficient versus blood concentration, a homogeneous liquid phantom was constructed using an 87-mm-diam plastic cup filled with 400-ml water solution of 1% intralipid. Figure 6 shows the absorption coefficient versus light wavelength and blood concentration change from 0 to 1%. The different marks in the plot correspond to the homogenous fits of absorption coefficient with six different wavelengths, and lines W1 through W6 are the fitted lines of measured absorption coefficients with wavelengths at 661, 761, 808, 826, and 849 nm, respectively. Equations on the right side of the figure show the slopes of these five fitted lines.

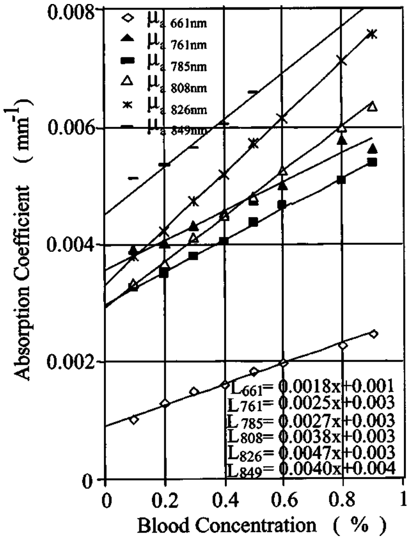

Fig. 6 Homogeneous fitted absorption coefficient versus blood concentration and light wavelength measured in a homogeneous liquid phantom. Lines S_{L1} through S_{L6} are the fits to the homogeneous absorption coefficient.

3.1 *Clinical Image Studies*

A 73-year-old female subject with a suspicious 3.5-cm left breast abnormality initially detected by mammography was imaged using our NIR imaging system. The mass location was determined by prior ultrasound examination immediately prior to the NIR imaging exam.[15] The source and detector fiber array was aligned approximately in the plane of the mass in a craniocaudal view of the breast (here called plane 1). The array was also placed in two other planes above and below the mass. Plane 0 was 13 mm toward the chest wall from the mass and plane 2 was 9 mm toward the nipple from the abnormality plane location. As a control image, the contralateral breast was also imaged in one plane at the approximate location of plane 1. Measurements in each plane were recorded at five wavelengths (661, 761, 785, 808, and 826 nm) and the images were reconstructed for absorption and reduced scattering coefficients.

We have shown detailed results of images from this patient, in three planes, with good correlation to the spatial location as determined by mammography and ultrasound images in a previous work.[15] Images of the total hemoglobin concentration in plane 1 of the left breast were reconstructed using the same patient data as in this previous work, but by reconstructing with different calibration phantoms (P1 through P6). These six images are shown in Fig. 7(a), where the location of the abnormality is readily observed slightly left of the middle in each image. The imaged plane diameter was 104 mm in this case. For comparison to a normal breast, Fig. 7(b) shows the image of total hemoglobin concentration of the contralateral breast in approximately the same plane from the chest wall. The abnormality in the left breast was subsequently removed and pathology confirmed the lesion as a ductal carcinoma. The average total hemoglobin concentration of the contralateral breast images was 17 to 19 μM, and the maximum total hemoglobin concentration in the center of the mass of the left breast was 47 to 49 μM. The variation in this maximum total hemoglobin concentration, induced when using different calibration phantoms including P1 through P6, was about 2% and the variation when using the best four of these calibration phantoms (i.e., P2 through P5) was only 1%.

Figure 7(c) shows the reduced scattering images with 785-nm light from both the symptomatic and contralateral breasts [corresponding to images in 7(a) and 7(b)]. Calibration phantoms P1 through P6 were used for the reconstruction. The average reduced scattering coefficient of the contralateral breast images was 0.98 mm^{-1}, and the maximum scattering coefficient in the center of the mass of the left breast was 1.7 to 1.8 mm^{-1}. The variation in this maximum scattering coefficient when using different phantoms (P1 through P6) to calibrate was about 3%.

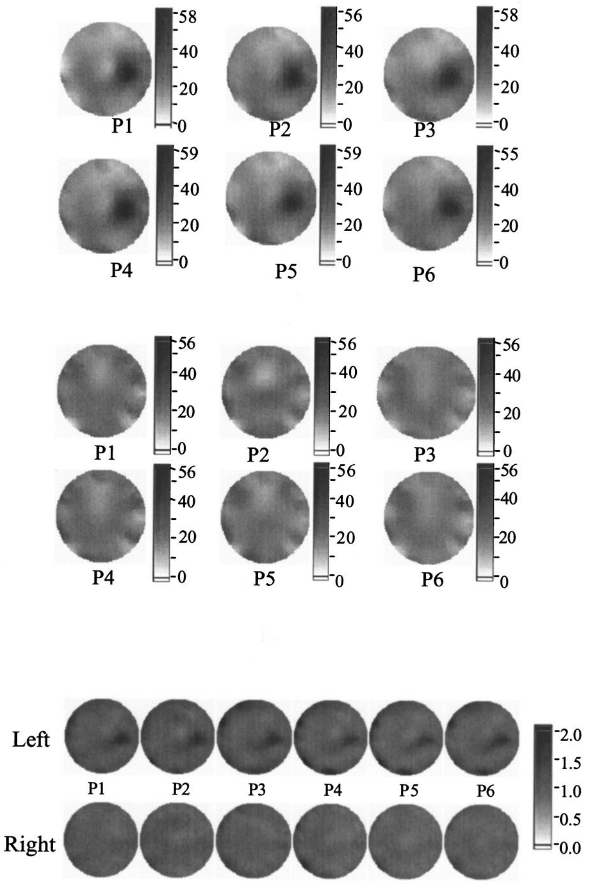

Fig. 7 Images of the total hemoglobin concentration of a patient breast obtained by using P1 through P6 homogenous calibration phantoms. (a) Left breast with a highly suspicious 3.5-cm mass initially detected by mammography. The imaged plane diameter is 104 mm. (b) Contralateral breast. The imaged plane diameter is 106 mm. (c) Scattering images with 785-nm light of both side of breast, reconstructed by using calibration phantoms P1 through P6.

4 Discussion

Evaluation of the performance of calibration phantoms is challenging in this type of nonlinear image reconstruction process, because it is not clear that the results obtained with any phantom is representative of all imaging situations. It is also not clear that imaging results obtained with phantoms can be directly applied to *in vivo* data where the background tissue is more heterogeneous and the fiber-tissue contact may cause different types of systematic artifacts to appear. In this study, a series of phantoms with different levels of contrast were used to examine imaging sensitivity to the reference phantom. A single localized region was used in the tissue-simulating test object because this situation mimics conditions we have experienced clinically where focal regions of high contrast are observed, due to increased total hemoglobin concentration within tumors. To address the tissue-contact issue, a set of hard and soft tissue-simulating phantoms was considered. The soft phantoms could be used to minimize artifacts in the image that are related to positioning errors in the fibers, because the fiber contact better matches the fiber-tissue interface when a breast is being examined.

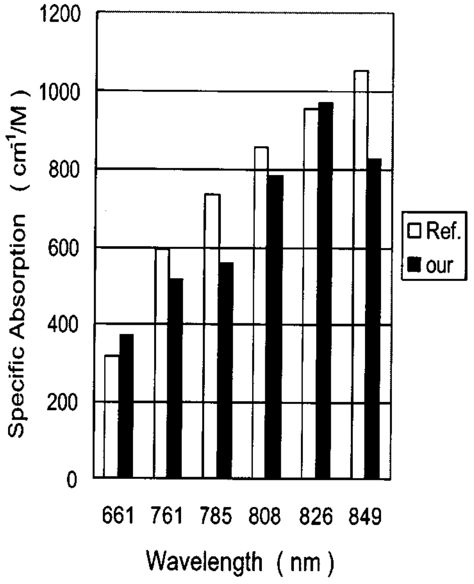

Fig. 8 The molar absorption coefficients of oxyhemoglobin as measured by the imaging system are shown along with values from Wray et al.[20]

From the slope of absorption coefficient versus blood concentration at each wavelength, the specific molar absorption can be estimated. Here we assume the oxygen saturation in our case was 100%. Figure 8 shows the specific absorption estimated from Fig. 6, and these results are compared with the data from Wray et al.[18] There is between 2 to 24% difference between these two datasets. Since the current system uses a tomographic approach to the quantitation of total hemoglobin rather than the standard spectrophotometric approach, we anticipate that the difference comes from minor model-data mismatch errors in the system. Further calibration is ongoing to determine if this difference can be minimized. However, the current working solution is to use molar absorption coefficients that have been measured on the imaging system, since they would help to eliminate systematic errors when calculating concentrations from images obtained in patients on this system.

Values for the slope of absorption coefficient versus blood concentration at a wavelength of 785 nm were compared between datasets taken from the large homogeneous solution (shown in Fig. 6) and the localized region (shown in Fig. 5) in a heterogeneous phantom. The localized region yields a value that is 15% lower than that measured in a large homogeneous phantom. The reason for this difference is likely related to a size effect, whereby the reconstructed target region is not fully recovered to the true peak value due to a blurring of the peak over the region. Further study of this effect and ways to minimize underestimation of the absorption coefficient of localized heterogeneities is ongoing.

A variation of 4% in the reconstructed scattering coefficient of all cases of different blood concentrations and by all P1 through P6 calibration phantoms occurs as the result of slight differences in the different homogenous fitting due to the effect of the calibration phantom size and optical properties.

When using a soft tissue-simulating calibration phantom, the data suggests that there is a benefit in reducing the image artifacts in the periphery of the imaging field. This can be seen in Fig.4, where high and low absorbing heterogeneities are located all around the periphery of the field, and near the source and detector positions. Conversely, using liquid phantoms (P6) appears to degrade the images, likely due to the fact that the sides of the bag are not sufficiently rigid to accurately mimic the shape of a breast in the array. Also, with the liquid phantoms, the presence of the plastic containment walls, which are transparent, may lead to lateral light channeling, which could give erroneous data at the distant detectors.[19] The soft phantoms were made of an RTV glue, which sets in a stiffness that is similar to breast tissue, and hence allows the fibers in the circular array to conform it into a similar shape as the breast being imaged.

In contrast, hard phantoms composed of inflexible resin will exhibit more differences in fiber position relative to the breast, because the rigidity of the resin stops the fibers as they are translated radially into the circular contact shape. Thus, the hard phantoms will have interfiber distance discrepancies that are not equal to those that occur when the breast tissue is in place. Boas et al.[20] have shown that very small distance errors on the order of 100 μm can lead to large phase shift and intensity errors. Hence, accurate repeatability of interfiber distances is likely a crucial element in minimizing image artifacts and improving image accuracy. From these results, it can be concluded that soft homogenous calibration phantoms have the advantage of reducing artifacts in the images due to the more uniform contact with the source and detector fiber optics.

5 Conclusions

The current near-infrared tomography system is being examined clinically to image total hemoglobin concentration and oxygen saturation within breast tissue. Optical projection measurements can be detected from tissue surfaces and combined with an appropriately designed diffusion model-based image reconstruction algorithm to recover maps of the tissue interior. To efficiently remove system offsets and obtain accurate initial estimates of the average optical properties of the breast, a homogenous phantom is used as a calibration between the data and the measurement system. By systematically examining the ability to quantify localized total hemoglobin concentrations, the response to different types of calibration phantoms has been evaluated. Using any of the six calibration phantoms deployed here led to a 3% standard deviation error in the slope of absorption coefficient versus total hemoglobin concentration. By carefully selecting soft homogeneous calibration phantoms, which are more uniformly in contact with the source and detector fiber optics, these variations can be reduced further to be about 1%. Tests of the system, based on reconstructed patient images with different homogenous calibration phantoms, indicate that the variation in the maximum total hemoglobin concentration value is less than 3% when using any of the six calibration phantoms. Using the soft homogeneous calibration phantom, this variation is further reduced to approximately 1% standard deviation error.

Acknowledgments

The authors would like to gratefully acknowledge the participation of Sandra Soho in the patient examination part of this study. This work has been funded by NCI grants PO1CA80139 and RO1CA69544.

References

1. B. Chance, Q. Luo, S. Nioka, D. C. Alsop, and J. A. Detre, ‘‘Optical investigations of physiology: a study of intrinsic and extrinsic biomedical contrast,’’ *Philos. Trans. R. Soc. London, Ser. B* **352**, 707–716 (1997).
2. M. A. Franceschini, K. T. Moesta, S. Fantini, G. Gaida, E. Gratton, H. Jess, W. W. Mantulin, M. Seeber, P. M. Schlag, and M. Kaschke, ‘‘Frequency-domain techniques enhance optical mammography: initial clinical results,’’ *Proc. Natl. Acad. Sci. U.S.A.* **94**(12), 6468–73 (1997).
3. B. J. Tromberg, O. Coquoz, J. B. Fishkin, T. Pham, E. R. Anderson, J. Butler, M. Cahn, J. D. Gross, V. Venugopalan, and D. Pham, ‘‘Noninvasive measurements of breast tissue optical properties using frequency-domain photon migration,’’ *Philos. Trans. R. Soc. London, Ser. B* **352**, 661–668 (1997).
4. B. W. Pogue, S. P. Poplack, T. O. McBride, W. A. Wells, O. K. S., U. L. Osterberg, and K. D. Paulsen, ‘‘Quantitative hemoglobin tomography with diffuse near-infrared spectroscopy: Pilot results in the breast,’’ *Radiology* **218**(1), 261–266 (2001).
5. B. W. Pogue, T. McBride, U. Osterberg, and K. Paulsen, ‘‘Comparison of imaging geometries for diffuse optical tomography of tissue,’’ *Opt. Express* **4**(8), 270–286 (1999).
6. B. W. Pogue, M. Testorf, T. McBride, U. Osterberg, and K. Paulsen, ‘‘Instrumentation and design of a frequency-domain diffuse optical tomography imager for breast cancer detection,’’ *Opt. Express* **1**(13), 391–403 (1997).
7. T. O. McBride, B. W. Pogue, U. L. Österberg, and K. D. Paulsen, ‘‘Strategies for absolute calibration of near infrared tomographic tissue imaging, in oxygen transport to tissue XXI,’’ J. F. Dunn, Swartz, H. M., Eds., Lengerich, Pabst (2001).
8. T. O. McBride, B. W. Pogue, S. Jiang, U. L. Osterberg, and K. D. Paulsen, ‘‘Development and calibration of a parallel modulated near-infrared tomography system for hemoglobin imaging *in vivo*,’’ *Rev. Sci. Instrum.* **72**(3), 1817–1824 (2001).
9. B. W. Pogue, K. D. Paulsen, H. Kaufman, and C. Abele, ‘‘Calibration of near infrared frequency-domain tissue spectroscopy for absolute absorption coefficient quantitation in neonatal head-simulating phantoms,’’ *J. Biomed. Opt.* **5**(2), 182–193 (2000).
10. T. D. Tosteson, B. W. Pogue, E. Demidenko, T. O. McBride, and K. D. Paulsen, ‘‘Confidence maps and confidence intervals for near infrared images in breast cancer,’’ *IEEE Trans. Med. Imaging* **18**(12), 1188–1193 (1999).
11. D. Boas, T. Gaudette, and S. Arridge, ‘‘Simultaneous imaging and optode calibration with diffuse optical tomography,’’ *Opt. Express* **8**(5), 263–70 (2001).
12. K. D. Paulsen and H. Jiang, ‘‘Spatially varying optical property reconstruction using a finite element diffusion equation approximation,’’ *Med. Phys.* **22**(6), 691–701 (1995).
13. B. W. Pogue, T. O. McBride, J. Prewitt, U. L. Osterberg, and K. D. Paulsen, ‘‘Spatially variant regularization improves diffuse optical tomography,’’ *Appl. Opt.* **38**(13), 2950–2961 (1999).
14. S. R. Arridge, ‘‘Optical tomography in medical imaging. Inverse probl.,’’ *Inverse Probl.* **15**(2), R41-R93 (1999).
15. T. O. McBride, B. W. Pogue, S. Jiang, U. L. Osterberg, K. D. Paulsen, and S. P. Poplack, ‘‘Multi-spectral near-infrared tomography: a case study in compensating for water and lipid content in hemoglobin imaging of the breast,’’ *J. Biomed. Opt.* **7**(1), 72–79 (2001).
16. T. O. McBride, B. W. Pogue, S. Jiang, U. L. Osterberg, K. D. Paulsen, and S. P. Poplack, ‘‘Initial studies of *in vivo* absorbing and scattering heterogeneity in near-infrared tomographic breast imaging,’’ *Opt. Lett.* **26**, 822–824 (2001).
17. T. O. McBride, B. W. Pogue, E. Gerety, S. Poplack, U. L. Osterberg, and K. D. Paulsen, ‘‘Preliminary study of near-infrared tomographic imaging of heterogeneous media: simulations and images of excised breast tissue,’’ *Proc. SPIE* **4250**, 204–210 (2001).

18. S. Wray, M. Cope, D. T. Delpy, J. S. Wyatt, and E. Reynolds, ''Charaterization of the near infrared absorption spectra of cytochrome aa_3 and haemoglobin for the non-invasive monitoring of cerebral oxygenation,'' *Biochem. Biophys. Acta* **933**, 184–192 (1988).
19. T. O. McBride, B. W. Pogue, E. Gerety, S. Poplack, U. L. Osterberg, and K. D. Paulsen, ''Spectroscopic diffuse optical tomography for quantitatively assessing hemoglobin concentration and oxygenation in tissue,'' *Appl. Opt.* **38**(25), 5480–5490 (1999).
20. D. A. Boas, M. A. O'Leary, B. Chance, and A. G. Yodh, ''Detection and characterization of optical in homogeneities with diffuse photon density waves: a signal-to-noise analysis,'' *Appl. Opt.* **36**, 75–92 (1997).